PCCP

ROYAL SOCIETY OF CHEMISTRY

PAPER

View Article Online
View Journal | View Issue

Cite this: *Phys. Chem. Chem. Phys.*, 2026, **28**, 10845

Rotational excitation and de-excitation of CP^- ($X^1\Sigma^+$) in collisions with He (^1S): cross-sections and rate coefficients

Liman Tian,[a] Tong Sun,[a] Chuangang Ning[b] and Xiaolin Chen *[a]

Received 12th March 2026,
Accepted 31st March 2026

DOI: 10.1039/d6cp00913a

rsc.li/pccp

Collisional energy transfer at low temperatures is crucial for astrophysical modeling. As an analogue to CN^-, the simplest interstellar anion detected to date, the phosphorus-bearing CP^- is a plausible candidate for astronomical searches. This paper investigates state-to-state rotational (de)-excitation of CP^- ($X^1\Sigma^+$) in collisions with He (^1S) over temperatures relevant to the cold interstellar medium and circumstellar envelopes. A new two-dimensional potential energy surface (PES) for the CP^-–He system was constructed within the rigid-rotor approximation using the CCSD(T) method extrapolated to the complete basis set (CBS) limit. The PES features a global minimum of -31.39 cm^{-1}. *Ab initio* points were fitted analytically with Legendre polynomials for quantum scattering calculations. Quantum close-coupling calculations were performed to obtain rotational inelastic cross-sections for rotational levels with $j \leq 10$ of CP^- at collision energies up to 1000 cm^{-1}. Resonances from quasi-bound states of the CP^-–He complex were present at low energies. By thermally averaging the cross-sections, we derived state-to-state rate coefficients ($k_{j\to j'}$) over the temperatures range 3–200 K for $\Delta j = \pm1, \pm2, \pm3$. The results indicate that dominant collision-induced transitions shift from $\Delta j = 1$ to $\Delta j = 2$ with increasing temperature. This work provides critical state-specific rotational rate coefficients for modeling CP^- abundance in the interstellar medium and for interpreting future astronomical observations seeking CP^-.

1. Introduction

The detection of molecular anions in the interstellar and circumstellar media marks a key advancement in understanding cosmochemistry.[1,2] Since the discovery of C_6H^- in 2006 by McCarthy,[3] a range of carbon-chain anions have been identified, including series of the form $C_{2n-1}N^-$ (n = 1–4) and $C_{2n}H^-$ (n = 2–5).[4–6] These findings confirm that anions are not only active participants in the astrochemical network[2] but also reveal significant uncertainties in existing models when predicting their abundance, primarily due to a lack of reliable baseline data on collisions with H_2 or He.[7] To fundamentally advance this field, it is crucial to extend research to more chemically diverse anions and to systematically quantify their collision processes.

Phosphorus-bearing molecules, including CP, PN, HCP, CCP, and others, are recognized as key carriers of interstellar phosphorus,[8] with unique significance for astrochemical research given the key role of phosphorus in the origin of life. Among them, the phosphorus-containing anion CP^- has become a highly valuable subject of study. As the smallest phosphorus-containing polar anion and the phosphorus-bearing analogue of the astronomically well-detected interstellar anion CN^-,[9] CP^- is an ideal template for exploring the physicochemical behavior of such species. Neutral CP has been definitively detected in carbon-rich circumstellar envelopes such as IRC + 10 216, with observed abundances of $\sim 1 \times 10^{-8}$ relative to H_2.[10] Its anionic counterpart, CP^-, is thus expected to exist in analogous astrochemical environments, with its existence inferred through mechanisms such as radiative electron attachment to HCP or dissociative electron attachment to precursor molecules.[11] Currently, the only available experimental data for CP^- come from negative ion photoelectron spectroscopy, which has yielded an electron affinity of 2.8508(7) eV,[12] while high-precision data concerning its equilibrium bond length, spectroscopic constants, and most critically its collisional rate coefficients remain unknown. This lack of data severely hinders the construction of astrochemical models and the evaluation of observational searches for CP^-.

Accurate abundance modeling and line profile simulation for CP^- demand precise state-to-state rotational (de)-excitation rate coefficients, $k_{j\to j'}$.[13,14] These coefficients are essential inputs for radiative transfer codes such as RADEX,[15] enabling accurate column density determination and the optimization of

[a] *College of Optical, Mechanical and Electrical Engineering, Zhejiang A&F University, 311300, Hangzhou, China. E-mail: chenxl13@zafu.edu*
[b] *Department of Physics, Tsinghua University, 100084, Beijing, China*

observational strategies with facilities like ALMA or JWST. The rate coefficients calculated in this paper will therefore serve as the key input parameters for future astrochemical models and for assessing the detectability of CP^-'s potential spectral lines. Moreover, based on its molecular properties, CP^- can be considered as a potentially effective electron reservoir in interstellar chemistry models and may play an important role in the chemical cycle of phosphorus.

Quantum scattering calculations of collision dynamics are available for several detected interstellar anions, including CN^-–He.[16–19] However, for the CP^-–He system, no such collisional data are currently available. Given that He is the second most abundant atom in the interstellar medium and is often used as a model collision partner for precise quantum scattering calculations to obtain benchmark data, considering the simpler internal structure of He atoms compared to H_2 molecules and the lower computational cost, this study first focuses on this collision system. To this end, this paper aims to provide, for the first time, the rotational inelastic collision cross-sections and rate coefficients for CP^- colliding with He at interstellar-related temperatures through high-precision quantum chemical calculations, laying the foundation for subsequent astrochemical modeling and observational searches. To address the lack of high-resolution spectroscopic data for CP^-, in Section 2, we compute its ground state $X^1\Sigma^+$ rotational constant, centrifugal distortion constant, and equilibrium bond length using the multi-reference configuration interaction (MRCI) method. We then construct a new *ab initio* PES for the CP^-–He system, expanded in Legendre polynomials. Section 3 details quantum scattering calculations using the close-coupling method to compute rotational excitation and de-excitation cross-sections and the subsequent thermal averaging to obtain rate coefficients in the temperature range 3–200 K. Finally, Section 4 will present our conclusions.

2. Methods

2.1. Diatomic constants for CP^-

The study of the CP^- ($X^1\Sigma^+$)–He (^1S) collision system primarily focuses on constructing a high-accuracy PES and its analytical fitting, which are essential for subsequent quantum scattering calculations. The vibrational frequency of CP^- ($X^1\Sigma^+$), as determined from negative ion photoelectron spectroscopy, is 1157(18) cm^{-1}.[12] Thus, collision energies up to 1000 cm^{-1} are insufficient to excite molecular vibrations. This justifies the use of the rigid rotor approximation. Furthermore, existing studies suggest that the cross-sections for vibrationally inelastic collisions are substantially smaller than those for rotational transitions,[20,21] further supporting the rigid-rotor approach. However, accurate experimental or theoretical data concerning the equilibrium bond length r_e, rotational constant B_0, and centrifugal distortion constant D_0 of ground-state CP^- are lacking in the existing literature. To address this gap, we compute these properties using high-accuracy *ab initio* methods. The equilibrium geometry of the CP^- ground state was optimized using the CCSD(T) method in conjunction with Dunning's correlation-consistent aug-cc-pVXZ (abbreviated aVXZ) (X = *T*, *Q*, 5)[22] basis sets for C[23] and P.[24] To approach the complete basis set (CBS) limit, a three-parameter extrapolation formula was employed:[25]

$$E_n = E_{CBS} + Be^{-(n-1)} + Ce^{-(n-1)2}, \quad (n = 3, 4, 5) \qquad (1)$$

where E_n is defined as the property calculated using a basis set with cardinal number n. E_{CBS} represents the extrapolated value at the CBS limit. Through this procedure, the CBS extrapolated equilibrium bond length is r_e = 1.6057 Å. Zou *et al.* extrapolated the equilibrium bond lengths of GaCl using the CBS formula. Their extrapolation results showed a high degree of consistency with the results obtained by refitting the extrapolated potential energy curve.[26,27] This finding strongly confirms the effectiveness and reliability of this extrapolation method.

To more accurately characterize the electronic structure of CP^- and determine its spectroscopic constants, we employed the multireference configuration interaction method with Davidson correction (MRCI+Q) with large Gaussian basis set aug-cc-pV5Z to provide the highest current accuracy for these method-sensitive derivative properties within manageable computational resources. All calculations utilized C_{2v} symmetry, a common approach for linear molecules in quantum chemistry packages that require Abelian point groups. The active space consisted of eight molecular orbitals (4 a_1, 2 b_1, 2 b_2), which primarily correspond to the valence 2s and 2p atomic orbitals of carbon and the 3s and 3p atomic orbitals of phosphorus. The remaining electrons were correlated in six closed-shell orbitals (4 a_1, 1 b_1, 1 b_2).

As shown in Fig. 1, the potential energy curve for the ground state was computed at 45 internuclear distances ranging from 1.2 to 7.0 Å. A finer step size of 0.05 Å was used near the equilibrium region to accurately capture the curvature of the potential well. The spectroscopic constants for the ground state of the CP^- ($X^1\Sigma^+$) were obtained from the potential energy curve

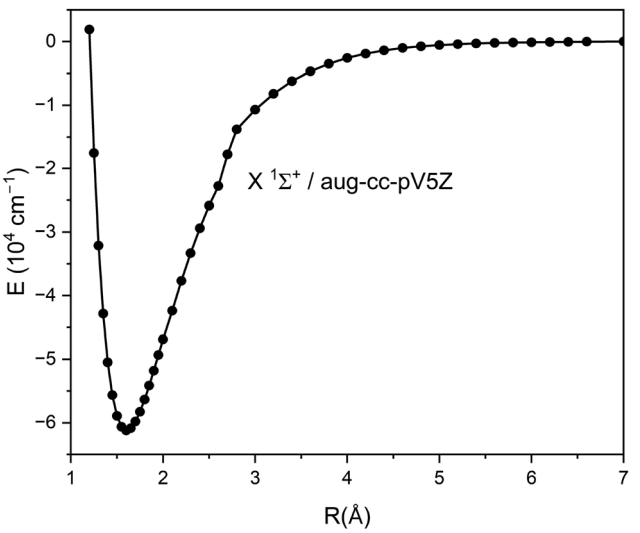

Fig. 1 MRCI+Q PES of CP^- ($X^1\Sigma^+$) using the aug-cc-pV5Z basis set.

using the VIBROT program of the OpenMolcas package,[28] yielding $B_0 = 0.75802\ cm^{-1}$ and $D_0 = 1.259 \times 10^{-6}\ cm^{-1}$. Our MRCI+Q method value of B_0 is in excellent agreement (within 0.25%) with the CCSD(T)/QFF result of $0.75992\ cm^{-1}$ from calculations[12] and within 1.03% of our own B3LYP/aV5Z result obtained using Gaussian 09.[29] Thus, we chose the MRCI+Q/aV5Z method to ensure high accuracy for these derivative-sensitive properties within manageable computational resources. Moreover, the equilibrium bond length fitted from MRCI+Q calculations (1.6028 Å) shows very close agreement with the CCSD(T)/CBS result (1.6057 Å), with a relative error within 0.2%, further confirming the reliability of our approach. These constants are essential for characterizing the rotational energy level structure of CP^-, which serves as direct input for the subsequent quantum scattering calculations of collision cross-sections.

2.2. Potential energy surface

The interaction PES was computed in Jacobi coordinates, as shown in Fig. 2, where R is the distance from the He atom to the center of mass of CP^-, and θ is the angle between the CP^- molecular axis and the vector **R** (with $\theta = 0^\circ$ corresponding to the He atom approaching the P atom). We sampled the PES over a wide grid, the intermolecular distance R was varied from 2.0 to 25.0 Å in steps of 0.1 Å, and the angle θ was varied from 0° to 180° in increments of 10°, yielding 19 distinct angular geometries. This grid ensures adequate coverage of the interaction region and convergence of the subsequent Legendre polynomial expansion. At each geometry, single-point energies are computed using the CCSD(T)/aVXZ method, and this method is reasonably applicable to phosphorus-containing molecules, such as HCCP,[30] CP,[31] and PN.[32] The CP^- bond length was fixed at the equilibrium value $r_e = 1.6057$ Å. In total, 4389 *ab initio* energy points were evaluated. All interaction energies, $V(R, \theta)$, were corrected for basis set superposition error (BSSE) using the standard counterpoise procedure[33] as given by

$$V(R, \theta) = E_{CP^-\text{–}He}(R, \theta) - E_{CP^-}(R, \theta) - E_{He}(R, \theta) \quad (2)$$

where $E_{CP^-\text{–}He}(R, \theta)$, $E_{CP^-}(R, \theta)$, and $E_{He}(R, \theta)$, are the total electronic energies of the CP^-–He, CP^- and He monomers, respectively.

To evaluate the performance of the CCSD(T)-F12A/aVTZ method for the CP^-–He system, we calculated one-dimensional potential energy curves along angular coordinates at $\theta = 0^\circ$, 90°, and 180°, respectively. The calculation results from three angles show a high degree of consistency. As shown in Fig. 3, the potential energy curve obtained using the CCSD(T)-F12A/aVTZ method shows a trend that is consistent with the limit results of the CBS. The CBS limit value is calculated using the traditional CCSD (T)/aVXZ method and extrapolated based on a three parameter exponential function. However, the relative errors of the CCSD(T)-F12A/aVTZ method in crucial regions of the potential are consistently in the range of 3–5%. This error margin substantially exceeds the typical tolerance required for high-accuracy quantum scattering calculations (generally $\leq$1%). Unlike the neutral HNSi/HSiN–He and HNC/HCN–Ar systems analyzed by Tian *et al.*,[34,35] where the long-range interaction is governed predominantly by dispersion forces, the present CP^-–He system is likely dominated by induced dipole interactions.

Based on this analysis, to ensure the reliability and numerical stability of subsequent scattering cross-section and rate coefficient calculations, we adopted the CBS-limit potential as the benchmark input. Although this choice entails higher computational cost, it effectively mitigates the uncertainty in scattering outcomes arising from inaccuracies in the potential energy surface, thereby aligning with the precision requirements of the present study. Analysis of the resulting two-dimensional PES, as shown in Fig. 4, reveals a global minimum located at $R = 4.508$ Å and $\theta = 116^\circ$, with a well depth of $31.39\ cm^{-1}$. The location of this minimum indicates that the He atom interacts most strongly near the carbon atom. All the *ab initio* calculations in this work are done using the MOLPRO program.[36]

2.3. Analytical representation

The two-dimensional PES $V(R, \theta)$ was expanded in a series of Legendre polynomials:

$$V(R, \theta) = \sum_{\lambda=0}^{\lambda_{max}} V_\lambda(R) P_\lambda(\cos\theta), \quad (3)$$

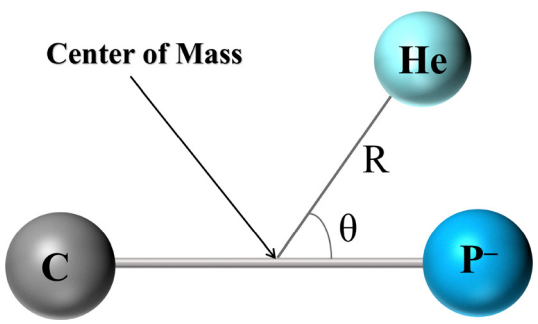

Fig. 2 Jacobi coordinates for the CP^- ($X^1\Sigma^+$)–He (^1S) collisional system.

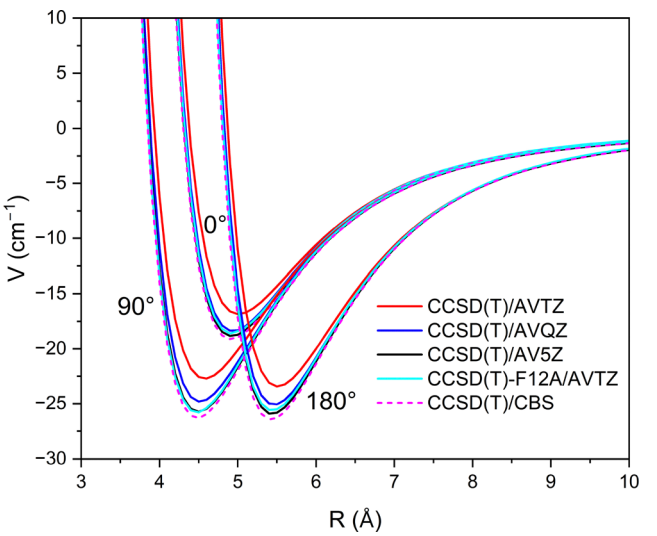

Fig. 3 Potential energy curves of the CP^-–He system for $\theta = 0^\circ$, 90°, 180°. The curves were calculated using CCSD(T)-F12A/aVTZ and CCSD(T)/aVXZ methods and CBS extrapolation.

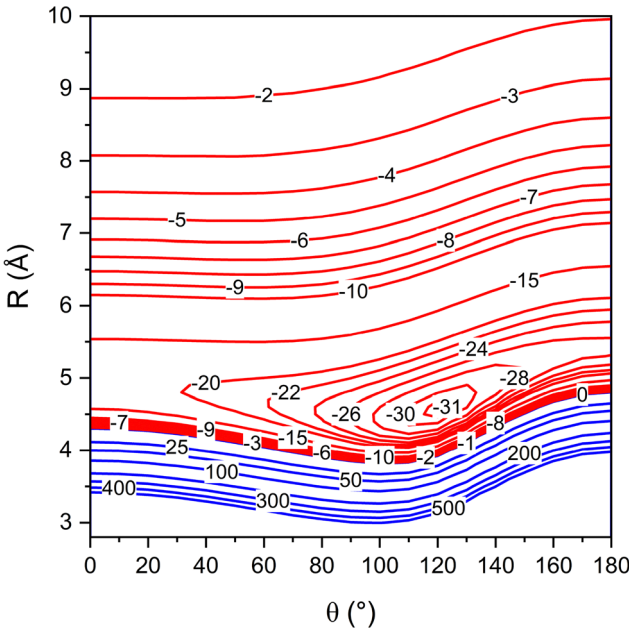

Fig. 4 Contour plots of the PESs for CP^-–He as functions of the intermolecular distance R and angular coordinate θ. Energy values are given in cm^{-1}. The negative energy regions are denoted by red contours, while the positive energy regions are represented by blue contours.

where $P_\lambda(\cos\theta)$ is the Legendre polynomial of order λ, and $V_\lambda(R)$ denotes the radial expansion coefficients. For each value of R, the coefficients $V_\lambda(R)$ are obtained numerically by exploiting the orthogonality of Legendre polynomials:

$$V_\lambda(R) = \frac{2\lambda+1}{2}\int_0^\pi V(R,\theta)P_\lambda(\cos\theta)\sin\theta\,\mathrm{d}\theta. \quad (4)$$

For the CP^-–He system, the expansion was truncated at λ_{max} = 18. This truncation level guarantees that the relative error between the analytical potential fit and the raw *ab initio* data remains below 0.5% across the entire interaction grid. Fig. 5 displays the variation of the radial coefficient $V_\lambda(R)$ with R. In the actual scattering calculation, 19 radial coefficients with $\lambda = 0 - 18$ were used. To clearly show the dominant characteristics of the lower-order terms, this figure only selects representative terms with $\lambda = 0 - 6$, which dominate the dynamical coupling between rotational states during the scattering process. We find that the anisotropic terms with $\lambda = 1$ and $\lambda = 2$ are the most significant ones. Consequently, the dynamical torque induced by these terms will preferentially drive direct rotational excitation processes with $\Delta j = 1$ and $\Delta j = 2$, as discussed in the scattering results section. This behavior is consistent with findings for CN^- colliding with He.[16]

An accurate analytical representation of $V_\lambda(R)$ over the full range of intermolecular distances is a prerequisite for quantum scattering calculations. Special attention must be paid to the precise fitting of the long-range region, as it dictates the appropriate asymptotic boundary conditions essential for reliable scattering results.

$$U_{ind}(R,\theta) = -\frac{1}{2}\frac{\alpha}{(4\pi\varepsilon_0)^2}\left(\frac{e^2}{R^4}+\frac{2\mu^2}{R^6}\right) - \frac{2e\mu\alpha}{R^5(4\pi\varepsilon_0)^2}\cos(\theta) - \frac{\alpha\mu^2}{2R^6(4\pi\varepsilon_0)^2}(3\cos^2(\theta)-1)+\cdots, \quad (5)$$

we analyzed the long-range part of the potential by comparing the *ab initio* values with the analytical induction model. For $\theta = 90°$, the expression is simplified to

$$U_{ind}(R,\theta=90°) = -\frac{\alpha}{2R^4} \quad (6)$$

As shown in Fig. 6, the CCSD(T)/CBS potential energy curves coincide almost exactly with the analytical $-\alpha/2R^4$ fit in the long-range region ($R > 10$ Å).

This indicates that the interaction in this range is dominated by the dipole-induced dipole induction, exhibiting the same R^{-4} asymptotic behavior as previously reported for the CF^+–He system.[37] The close agreement between the *ab initio* results and

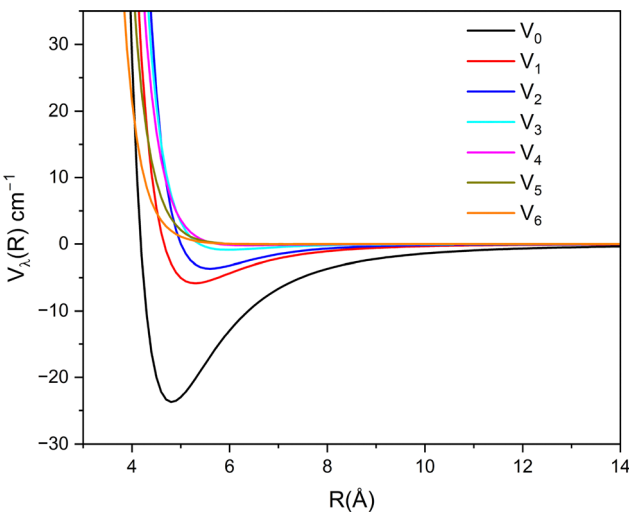

Fig. 5 $V_\lambda(R)$ terms as a function of R for the value of λ up to 6.

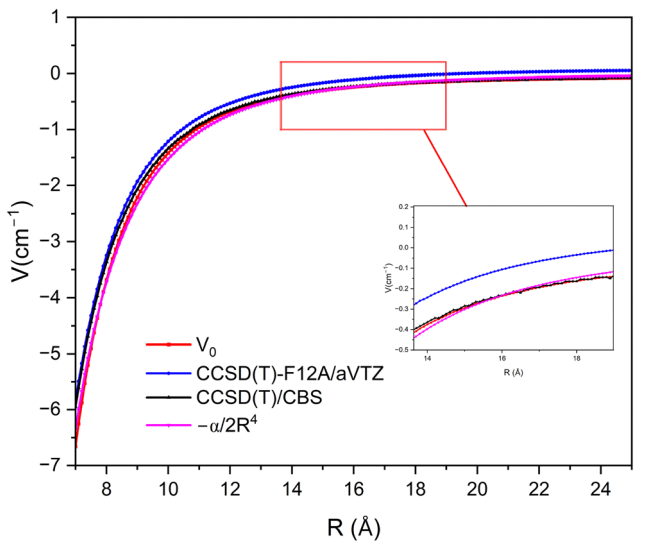

Fig. 6 Comparison between the long-range *ab initio* and analytical potential energies of the CP^-–He system for $\theta = 90°$.

the simple induction form confirms that the long-range tail of the potential is physically well described, providing a reliable foundation for subsequent quantum scattering calculations, particularly for the accurate prediction of low-temperature rate coefficients.

3. Scattering calculations and collisional properties

3.1. Cross-sections

To investigate the quantum dynamics of inelastic scattering in the CP^-–He system, we employ the close coupling (CC) method, proposed by Arthurs.[38] The Hamiltonian in Jacobian coordinates is expressed as:

$$H = -\frac{\hbar^2}{2\mu}R^{-1}\frac{d^2}{dR^2}R + \frac{\hbar^2\hat{L}^2}{2\mu R^2} + H_{\text{internal}}(\xi_{\text{internal}}) + V(R, \xi_{\text{internal}}) \tag{7}$$

where μ is the reduced mass of the collision complex, $\hat{L}$ represents the angular momentum operator, R represents the distance between the He atom and the CP^- center of mass, ξ_{internal} represents the internal coordinates of the molecule, and H_{internal} represents the internal Hamiltonian of the molecule. The interaction potential $V(R, \xi_{\text{internal}})$ is described by the newly constructed PES.

$$\Psi(R, \xi_{\text{internal}}) = R^{-1}\sum_b \Phi_b(\xi_{\text{internal}})\psi_b(R) \tag{8}$$

To solve the molecular scattering problem, we decompose the total wave function according to eqn (8): the complete basis functions $\Phi_b(\xi_{\text{internal}})$ describing the molecular rotational dynamics form an orthogonal normalized set, whose expansion coefficients are the radial wave function $\psi_b(R)$ to be determined. Substituting this decomposition into the Schrödinger equation and projecting it onto each basis function, we finally obtain a set of coupled radial equations.[13]

$$\frac{d^2\psi_a}{dR^2} = \sum_b [W_{ab}(R) - \varepsilon\delta_{ab}]\psi_b(R) \tag{9}$$

where $\varepsilon = 2\mu E/h^2$, δ_{ab} is the Kronecker δ, and when $a \neq b$, the coupling matrix element $W_{ab}(R)$ is given by the following equation:

$$W_{ab}(R) = \frac{2\mu}{\hbar^2}\int \Phi_a^*(\xi_{\text{internal}})\left[\frac{\hbar^2\hat{L}^2}{2\mu R^2} + H_{\text{internal}} + V(R, \xi_{\text{internal}})\right] \times \Phi_b(\xi_{\text{internal}})d\xi_{\text{internal}} \tag{10}$$

The coupled equations in matrix form can be expressed as follows:

$$\frac{d^2\psi}{dR^2} = [\boldsymbol{W}(R) - \varepsilon\boldsymbol{I}]\psi(R) \tag{11}$$

These coupling equations will be solved numerically using the molscat package.[13] In this computational framework, $\boldsymbol{I}$ represents the identity matrix, and $\boldsymbol{W}(R)$ represents the interaction matrix, whose elements are defined as $W_{ab}(R)$. The core input to the program is the fitted radial expansion coefficients $V_\lambda(R)$.

We applied by coupling the analytically fitted anisotropic PES into the coupled-channel equations to compute integral cross sections for transitions among the first 11 ($j \leq 10$) rotational states of CP^-. The modified log-derivative method of Manolopoulos (LDMD) and the Airy propagator were employed to solve the coupled equations, handling the short-range and long-range interactions, respectively.[39,40]

The rotational energy levels of the system are given by

$$E_j = B_0 j(j+1) - D_0[j(j+1)]^2 \tag{12}$$

where B_0 and D_0 are taken from our computational results above. The integral cross-section from initial rotational state j to final state j' is obtained from the scattering matrix elements $S^J_{jj'll'}$:

$$\sigma_{j\to j'}(E_k) = \frac{\pi}{k_j^2(2j+1)}\sum_{J=0}\sum_{l=|J-j|}^{J+j}\sum_{l'=|J-j'|}^{J+j'} \times(2J+1) \times \left|\delta_{jj'}\delta_{ll'} - S^J_{jj'll'}(E)\right|^2, \tag{13}$$

where $k_j = \sqrt{2\mu(E-E_j)}/\hbar$ is the wavenumber, μ is the reduced mass of the CP^-–He system, E_j is the energy of rotational level j, E is the total energy, and l, l' denote the initial and final orbital angular momentum quantum numbers, respectively.

To achieve convergence with a relative error below 0.5% in the cross-sections for rotational levels up to $j = 10$, the rotational basis size was varied with energy: $J_{max} = 14$ for $E \leq 100$ cm^{-1}, $J_{max} = 17$ for 100 cm^{-1}, $E \leq 300$ cm^{-1}, $J_{max} = 20$ for 300 cm^{-1}, $E \leq 500$ cm^{-1}, and $J_{max} = 25$ for 500 cm^{-1}, $E \leq 1000$ cm^{-1}. A non-uniform energy grid was employed to accurately resolve the resonance structures in the cross-sections, which is critical for obtaining correct rate coefficients. The grid step size was 0.1 cm^{-1} for 0.1–100 cm^{-1}, 1.0 cm^{-1} for 100–300 cm^{-1}, 5 cm^{-1} for 300–500 cm^{-1}, and 20 cm^{-1} for 500–1000 cm^{-1}.

Fig. 7(a) and (b) present the cross-sections for rotational excitation ($\Delta j = +1, +2, +3$) and de-excitation ($\Delta j = -1, -2, -3$) as a function of collision energy, respectively. At low collision energies ($E \leq 30$ cm^{-1}), both Fig. 7(a) and (b) exhibit numerous resonance structures, attributable to Feshbach resonances associated with quasi bound states and shape resonances near the threshold in the effective potential. These resonant features are gradually damped with increasing energy, and the cross-sections evolve towards a smoother, declining trend. In particular, as shown in Fig. 7(a), the excitation cross-section with $\Delta j = 1$ dominates in the low-energy region and decreases monotonically with increasing energy. The cross-section with $\Delta j = 2$ lacks the sharp resonance peaks visible in the low-energy region about 20 cm^{-1}. The de-excitation cross section, shown in Fig. 7(a), shows a similar trend. By contrast, the $\Delta j = \pm 3$ cross-sections are smaller by 1–2 orders of magnitude relative to $\Delta j = \pm 1, \pm 2$ over the entire energy range. It is noteworthy that de-excitation processes such as $\Delta j = -2$ are comparatively larger 10–100 cm^{-1}, whereas specific excitation processes such as $0 \to 2$, $1 \to 3$, $2 \to 4$, and $3 \to 5$ ($\Delta j = +2$) experience a significant enhancement above 300 cm^{-1}. This

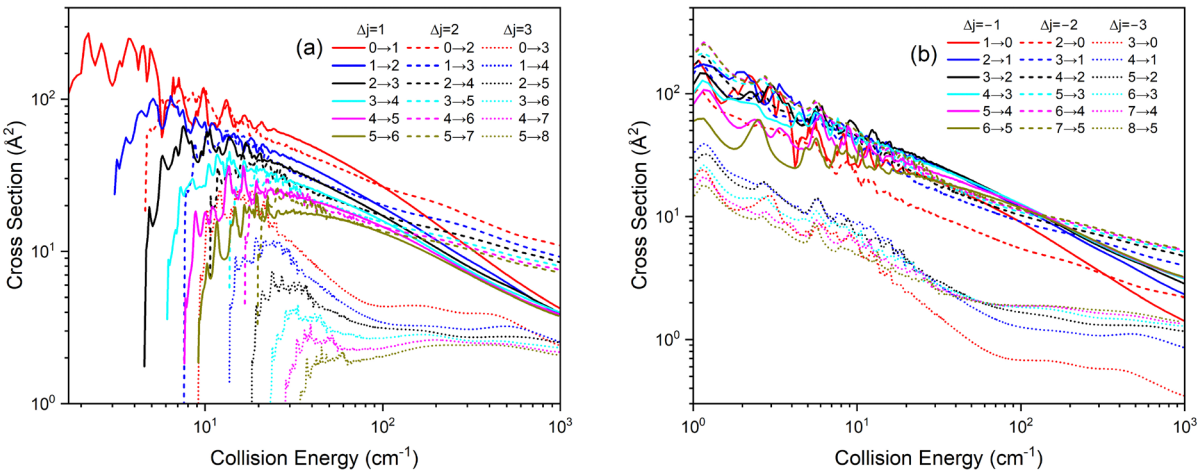

Fig. 7 Rotational state-to-state cross-sections in CP^-–He collisions: (a) excitation and (b) de-excitation *versus* collision energy.

energy-dependent propensity is governed by the contributions of the anisotropic terms in the potential: transitions with $\Delta j = 1$ in the low-energy region are primarily mediated by the V_1 term, whereas those with $\Delta j = 2$ in the high-energy region are more influenced by the V_2 term. This behavior is consistent with that reported for the CN^-–He system,[16] where $\Delta j = \pm 1$ transitions dominate at low energies and the role of $\Delta j = \pm 2$ becomes increasingly prominent at higher energies.

3.2. Rate coefficients

For application in astrochemical modeling, the cross-sections were thermally averaged to obtain the rate coefficients. The rate coefficient $k_{j\to j'}(T)$ is calculated by:

$$k_{j\to j'}(T) = \left(\frac{8}{\pi\mu k_B{}^3 T^3}\right)^{1/2} \times \int_0^\infty E_k \sigma_{j\to j'}(E_k) e^{-E_k/k_B T} dE_k, \quad (14)$$

where k_B is the Boltzmann constant, μ is the reduced mass of the CP^-–He system, and $\sigma_{j\to j'}(E_k)$ is the energy-dependent cross-section.

Fig. 8(a) and (b) show the excitation and de-excitation rate coefficients in the temperature range of 3–200 K, including transitions with $\Delta j = \pm 1, \pm 2, \pm 3$. As shown in Fig. 8(a), at temperatures below 100 K, for the same initial energy level j, transitions with $\Delta j = 1$ dominate, while above this temperature, transitions show a preference for $\Delta j = 2$. The de-excitation process is different. As shown in Fig. 8(b), when the initial energy level j is less than 4, for the same initial energy level, transitions with $\Delta j = -1$ dominate throughout the temperature range, and the rate coefficient for the $3 \to 2$ transition reaches a peak of approximately 1.2×10^{-10} cm^3 $molecule^{-1}$ s^{-1} near 12 K. When the initial energy level $j > 4$, for the same initial energy level, a de-excitation process with $\Delta j = -2$ briefly dominates at low temperatures. This trend strengthens across the entire temperature range as the initial energy level j continues to increase. When the initial energy level j is sufficiently large, such as $j = 6$, the $6 \to 5$ transition is generally higher than the $6 \to 4$ transition. The rate coefficient for the $7 \to 5$ transition reaches approximately 0.9×10^{-10} cm^3 $molecule^{-1}$ s^{-1} at 100 K, which is on the same order

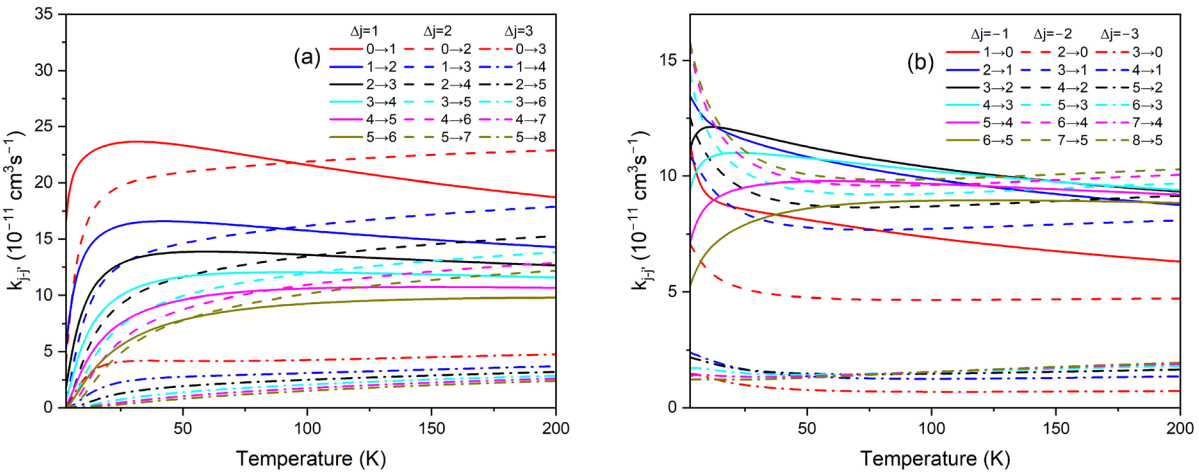

Fig. 8 Rotational state-to-state rate coefficients for CP^-–He as a function of temperature: (a) excitation and (b) de-excitation.

of magnitude as the 7 → 5 transition rate coefficient in the CN^-–He system.[16]

The rate coefficients for $\Delta j = \pm 3$ transitions are typically an order of magnitude smaller than those for $\Delta j = \pm 1$, ± 2 and become negligible below 20 K. These rate coefficients provide critical input data for non-LTE spectral modeling of CP^- in the interstellar medium. Based on these results, we propose observational strategies: in typical molecular clouds ($T > 10$ K), priority should be given to detecting $\Delta j = -1$ transitions, particularly 3 → 2 and 2 → 1; in warmer environments (*e.g.*, protostellar envelopes, $T > 70$ K), greater attention should be paid to $\Delta j = -2$ transitions such as 7 → 5 and 6 → 4, as their rate coefficients exceed those of some $\Delta j = -1$ channels at certain temperatures. The temperature dependence of the rate coefficients follows characteristic patterns: the $\Delta j = 1$ rates decrease with increasing temperature below ∼20 K (due to diminishing resonance contributions) and increase monotonically above ∼20 K; the $\Delta j = 2$ rates exhibit continuous growth throughout the 3–200 K range, which is the characteristic of higher-energy processes requiring more kinetic energy to become efficient.

However, it is important to emphasize that this study aims to obtain collision data (including radial coefficients, rate coefficients, *etc.*) for the CP^-–He system, rather than directly providing CP^-–H_2 collision data suitable for non-LTE radiative simulations. In fact, due to the significant difference in the anisotropy of their potential energy surfaces, even estimating CP^-–H_2 collision results through reduced mass scaling will introduce considerable uncertainty. Instead, the significance of this study lies in its fundamental exploration, constructing a preliminary theoretical framework for the collision dynamics of CP^- molecules and providing crucial input parameters and a research foundation for future accurate radiative transfer simulations based on H_2 collisions.

4. Conclusion

This work reports the first systematic investigation of rotational (de)-excitation in the CP^-–He system based on quantum scattering calculations. CP^-, as the phosphorus analogue of CN^-, is a promising interstellar anion whose abundance could be non-negligible in C-rich circumstellar envelopes such as IRC + 10 216; therefore, obtaining the accurate collision rate coefficient of CP^- becomes necessary. Our results are summarized as follows: the computed PES is characterized by a global minimum of -31.39 cm^{-1} at $R = 4.508$ Å and $\theta = 116^\circ$, exhibiting a distinct topology compared to systems like CN^-–He. Pronounced resonance structures in the low-energy region (<30 cm^{-1}) lead to a dramatic enhancement of the $\Delta j = 1$ cross-sections. These resonances are attributed to quasi bound states of the transient CP^-–He complex. The state-to-state rate coefficients display a marked temperature dependence: de-excitation processes with $\Delta j = -1$ are dominant at low temperatures ($T < 100$ K), while those with $\Delta j = -2$ gain prominence at higher temperatures ($T > 100$ K). The fact that the rate coefficients for CP^- are of the same order of magnitude as those of its analogue, CN^-, supports the physical intuition that such closed-shell anions exhibit broadly comparable collisional behavior with He. However, the primary goal of this work is to establish the first and definitive dataset for CP^- itself, which now enables its inclusion in astrochemical models. For astrochemical modelling and observational purposes, we propose to prioritize the search for the 2 → 1 transition in cold molecular clouds and to target $\Delta j = -2$ transitions, such as 7 → 5, in warmer regions.

The present collisional data provided the only accurate reference for validating approximation methods in any subsequent H_2 collision calculations and obtained critical input parameters for non-LTE radiative transfer modelling of phosphorus-bearing anions in the interstellar medium, thereby helping to constrain the phosphorus chemical cycle. Future work will be extended to include calculations for CP^-–H_2 collisions, as well as a study of isotopic variants (*e.g.*, $^{13}CP^-$), which are crucial for interpreting future astronomical observations.

Author contributions

Liman Tian: investigation (lead); writing – original draft (lead); writing – review & editing (lead). Tong Sun: investigation (supporting). Chuangang Ning: investigation (supporting); resources (lead). Xiaolin Chen: investigation (lead); writing – original draft (lead); supervision (lead); writing – review & editing (lead). All authors discussed the results and contributed to the final manuscript.

Conflicts of interest

There are no conflicts to declare.

Data availability

The data supporting this article are included as part of the supplementary information (SI). Supplementary information: values of rotationally inelastic excitation and de-excitation of cross-sections and rate coefficients for the CP^-–He system, supplied in numerical form. See DOI: https://doi.org/10.1039/d6cp00913a.

Acknowledgements

This work was supported by the National Natural Science Foundation of China (NSFC) (Grant No. 12374244 and 12341401) and the Scientific Research Development Fund Project of the Zhejiang A&F University (Grant No. 2024LFR048).

References

1 R. C. Fortenberry, *J. Phys. Chem. A*, 2015, **119**, 9941–9953.
2 T. J. Millar, C. Walsh and T. A. Field, *Chem. Rev.*, 2017, **117**, 1765–1795.

3 M. C. McCarthy, C. A. Gottlieb, H. Gupta and P. Thaddeus, *Astrophys. J., Lett.*, 2006, **652**, L141–L144.
4 B. A. McGuire, *Astrophys. J., Suppl. Ser.*, 2022, **259**, 30.
5 J. Cernicharo, J. Pardo, C. Cabezas, M. Agúndez, B. Tercero, N. Marcelino, R. Fuentetaja, M. Guélin and P. de Vicente, *Astron. Astrophys.*, 2023, **670**, L19.
6 J. R. Pardo, C. Cabezas, M. Agúndez, B. Tercero, N. Marcelino, P. de Vicente, M. Guélin and J. Cernicharo, *Astron. Astrophys.*, 2023, **677**, A55.
7 E. Roueff and F. Lique, *Chem. Rev.*, 2013, **113**, 8906–8938.
8 J. Chantzos, V. M. Rivilla, A. Vasyunin, E. Redaelli, L. Bizzocchi, F. Fontani and P. Caselli, *Astron. Astrophys.*, 2020, **633**, A54.
9 M. Agúndez, J. Cernicharo, M. Guélin, C. Kahane, E. Roueff, J. Klos, F. J. Aoiz, F. Lique, N. Marcelino, J. R. Goicoechea, M. González García, C. A. Gottlieb, M. C. McCarthy and P. Thaddeus, *Astron. Astrophys.*, 2010, **517**, L2.
10 S. N. Milam, D. T. Halfen, E. D. Tenenbaum, A. J. Apponi, N. J. Woolf and L. M. Ziurys, *Astrophys. J.*, 2008, **684**, 618–625.
11 M. Agúndez, J. Cernicharo and M. Guélin, *Astrophys. J., Lett.*, 2007, **662**, L91–L94.
12 J. Czekner, L. F. Cheung, E. L. Johnson, R. C. Fortenberry and L.-S. Wang, *J. Chem. Phys.*, 2018, **148**, 044301.
13 J. M. Hutson and C. R. Le Sueur, *Comput. Phys. Commun.*, 2019, **241**, 9–18.
14 M. H. Alexander, P. J. Dagdigian, H. J. Werner, J. Klos, B. Desrousseaux, G. Raffy and F. Lique, *Comput. Phys. Commun.*, 2023, **289**, 108761.
15 F. F. S. van der Tak, J. H. Black, F. L. Schöier, D. J. Jansen and E. F. van Dishoeck, *Astron. Astrophys.*, 2007, **468**, 627–635.
16 L. González-Sánchez, B. P. Mant, R. Wester and F. A. Gianturco, *Astrophys. J.*, 2020, **897**, 1.
17 B. Mant, E. Yurtsever, L. González-Sánchez, R. Wester and F. A. Gianturco, *J. Chem. Phys.*, 2021, **154**, 084305.
18 C. Lochmann, S. P. Melath, R. Wild, E. Yurtsever, A. Martín Santa Daría, L. González-Sánchez, F. A. Gianturco and R. Wester, *Astrophys. J.*, 2024, **976**, 114.
19 L. González-Sánchez, A. M. S. Daría, E. Yurtsever, F. A. Gianturco, C. Lochmann and R. Wester, *Mon. Not. R. Astron. Soc.*, 2025, **539**, 3722–3731.
20 A. Faure, P. Valiron, M. Wernli, L. Wiesenfeld, C. Rist, J. Noga and J. Tennyson, *J. Chem. Phys.*, 2005, **122**, 221102.
21 T. Stoecklin, O. Denis-Alpizar, A. Clergerie, P. Halvick, A. Faure and Y. Scribano, *J. Phys. Chem. A*, 2019, **123**, 5704–5712.
22 T. H. Dunning, *J. Chem. Phys.*, 1989, **90**, 1007–1023.
23 R. A. Kendall, T. H. Dunning and R. J. Harrison, *J. Chem. Phys.*, 1992, **96**, 6796–6806.
24 D. E. Woon and T. H. Dunning, *J. Chem. Phys.*, 1993, **98**, 1358–1371.
25 K. A. Peterson, D. E. Woon and T. H. Dunning, *J. Chem. Phys.*, 1994, **100**, 7410–7415.
26 D. Deng, Y. Lian and W. Zou, *Chem. Phys. Lett.*, 2017, **688**, 33–36.
27 Y. Fu, Y. Niu, X. Liang, H. Liu and W. Zou, *J. Phys. Chem. A*, 2022, **126**, 5565–5573.
28 F. Aquilante, J. Autschbach, A. Baiardi, S. Battaglia, V. A. Borin, L. F. Chibotaru, I. Conti, L. De Vico, M. Delcey and N. Ferré, *et al.*, *J. Chem. Phys.*, 2020, **152**, 214117.
29 M. Frisch, *Gaussian 09, Revision d. 01*, Gaussian, 2009.
30 T. Dhilip Kumar, *Mon. Not. R. Astron. Soc.*, 2022, **515**, 5145–5150.
31 C. T. Bop, N. Boye Faye, K. Hammami and N. Jadane, *J. Phys. Chem. A*, 2017, **121**, 7854–7860.
32 R. Toboła, J. Kłos, F. Lique, G. Chałasinski and M. Alexander, *Astron. Astrophys.*, 2007, **468**, 1123–1127.
33 S. F. Boys and F. Bernardi, *Mol. Phys.*, 1970, **19**, 553–566.
34 L. Tian, T. Sun, C. Ning and X. Chen, *Chin. J. Chem. Phys.*, 2026, 1–10.
35 L. Tian, T. Sun, W. Zou and X. Chen, *Mon. Not. R. Astron. Soc.*, 2026, **545**, 1–9.
36 H. Werner, P. J. Knowles, G. Knizia, F. R. Manby and M. Schütz, *Wiley Interdiscip. Rev.: Comput. Mol. Sci.*, 2012, **2**, 242–253.
37 Y. Ajili and K. Hammami, *Astron. Astrophys.*, 2013, **556**, A82.
38 A. Arthurs and A. Dalgarno, *Proc. R. Soc. London, Ser. A*, 1960, **256**, 540–551.
39 M. H. Alexander, *J. Chem. Phys.*, 1984, **81**, 4510–4516.
40 M. H. Alexander and D. E. Manolopoulos, *J. Chem. Phys.*, 1987, **86**, 2044–2050.

